



## OPEN ACCESS

## EDITED BY

Gang Wu,  
VU Amsterdam, Netherlands

## REVIEWED BY

Roy Morello,  
University of Arkansas for Medical  
Sciences, United States  
Brya Matthews,  
The University of Auckland, New Zealand

## \*CORRESPONDENCE

Chao Yang,  
✉ zhangxiuyc@sina.com  
Zhongquan Dai,  
✉ daizhq77@163.com  
Yinghui Li,  
✉ yinghuidd@vip.sina.com

<sup>†</sup>These authors have contributed equally  
to this work and share first authorship

## SPECIALTY SECTION

This article was submitted  
to Skeletal Physiology,  
a section of the journal  
Frontiers in Physiology

RECEIVED 03 January 2023

ACCEPTED 20 March 2023

PUBLISHED 28 March 2023

## CITATION

Xu Z, Yang C, Wu F, Tan X, Guo Y,  
Zhang H, Wang H, Sui X, Xu Z, Zhao M,  
Jiang S, Dai Z and Li Y (2023), Triple-gene  
deletion for osteocalcin significantly  
impairs the alignment of hydroxyapatite  
crystals and collagen in mice.  
*Front. Physiol.* 14:1136561.  
doi: 10.3389/fphys.2023.1136561

## COPYRIGHT

© 2023 Xu, Yang, Wu, Tan, Guo, Zhang,  
Wang, Sui, Xu, Zhao, Jiang, Dai and Li. This  
is an open-access article distributed  
under the terms of the [Creative  
Commons Attribution License \(CC BY\)](#).  
The use, distribution or reproduction in  
other forums is permitted, provided the  
original author(s) and the copyright  
owner(s) are credited and that the original  
publication in this journal is cited, in  
accordance with accepted academic  
practice. No use, distribution or  
reproduction is permitted which does not  
comply with these terms.

# Triple-gene deletion for osteocalcin significantly impairs the alignment of hydroxyapatite crystals and collagen in mice

Zihan Xu<sup>1,2†</sup>, Chao Yang<sup>2†\*</sup>, Feng Wu<sup>2†</sup>, Xiaowen Tan<sup>3</sup>, Yaxiu Guo<sup>2</sup>, Hongyu Zhang<sup>2</sup>, Hailong Wang<sup>2</sup>, Xiukun Sui<sup>2</sup>, Zi Xu<sup>2</sup>, Minbo Zhao<sup>3</sup>, Siyu Jiang<sup>1</sup>, Zhongquan Dai<sup>2\*</sup> and Yinghui Li<sup>1,2\*</sup>

<sup>1</sup>School of Life Science and Technology, Harbin Institute of Technology, Harbin, China, <sup>2</sup>State Key Laboratory of Space Medicine Fundamentals and Application, China Astronaut Research and Training Center, Beijing, China, <sup>3</sup>Department of Pathology and Forensics, Dalian Medical University, Dalian, China

Osteocalcin (Ocn), also known as bone Gla protein, is synthesized by osteoblasts and thought to regulate energy metabolism, testosterone synthesis and brain development. However, its function in bone is not fully understood. Mice have three Ocn genes: Bglap, Bglap2 and Bglap3. Due to the long span of these genes in the mouse genome and the low expression of Bglap3 in bone, researchers commonly use Bglap and Bglap2 knockout mice to investigate the function of Ocn. However, it is unclear whether Bglap3 has any compensatory mechanisms when Bglap and Bglap2 are knocked out. Considering the controversy surrounding the role of Ocn in bone, we constructed an Ocn-deficient mouse model by knocking out all three genes (Ocn<sup>-/-</sup>) and analyzed bone quality by Raman spectroscopy (RS), Scanning electron microscopy (SEM), Fourier transform infrared spectroscopy (FTIR) and MicroCT ( $\mu$ CT). The RS test showed that the alignment of hydroxyapatite crystals and collagen fibers was significantly poorer in Ocn<sup>-/-</sup> mice than in wild-type (WT) mice. Ocn deficiency resulted in a looser surface structure of bone particles and a larger gap area proportion. FTIR analysis showed few differences in bone mineral index between WT and Ocn<sup>-/-</sup> mice, while  $\mu$ CT analysis showed no significant difference in cortical and trabecular regions. However, under tail-suspension simulating bone loss condition, the disorder of hydroxyapatite and collagen fiber alignment in Ocn<sup>-/-</sup> mice led to more obvious changes in bone mineral composition. Collectively, our results revealed that Ocn is necessary for regulating the alignment of minerals parallel to collagen fibrils.

## KEYWORDS

osteocalcin, collagen fiber arrangement, bone mineral composition, bone microstructure, tail suspension

## 1 Introduction

Bone is a biomineralized composite composed of collagen, non-collagenous proteins (NCPs) and carbonate-substituted hydroxyapatite minerals (López Barreiro et al., 2022). Among the bone matrix, osteocalcin (Ocn) is one of the most abundant NCPs. Other major types of NCPs are osteonectin (ON), fibronectin (FN), and osteopontin (OPN) (Hauschka et al., 1989). Unlike these proteins, osteocalcin is a bone-specific protein mainly produced by

osteoblasts during bone formation and is found deep in the densely mineralized region of cortical bone (Weinreb et al., 1990; Chenu et al., 1994).

In humans and rats, Ocn is encoded by a single gene (*BGLAP*) (Li et al., 1995). While in mice, there are three genes: *Bglap*, *Bglap2*, which are highly expressed in bone; and *Bglap3*, which is mainly expressed in the kidney (Desbois et al., 1994). Post-translational  $\gamma$ -carboxylation carried out by  $\gamma$ -glutamyl carboxylase (GGCX) is one of the critical features of Ocn. During carboxylation, a second carboxyl group is added to specific glutamyl residues (Glu) at positions 17, 21, and 24 forming  $\gamma$ -carboxyglutamyl residues (Gla). This modification leads to a conformational change, stabilizing the  $\alpha$ -helical portion of the protein and conferring a greater affinity for calcium and hydroxyapatite (Lee et al., 2000). Because of these structural features, Ocn is thought to play an essential role in bone mineralization processes and hydroxyapatite growth (Hoang et al., 2003). Meanwhile, Ocn is also often used as an indicator of bone turnover, which has been justified by the necessity of preserving the mechanical integrity of the skeleton and regulating calcium and phosphorus homeostasis (Lian and Gundberg, 1988; McGuigan et al., 2010).

Based on the Ocn deficient mice generated by simultaneously deleting both *Bglap* and *Bglap2* genes, Ducy P., found that a lack of Ocn leads to an increase in bone formation without impairing bone resorption. However, this knockout of Ocn did not affect bone mineralization. Furthermore, female Ocn-deficient mice were resistant to oophorectomy-induced bone loss (Ducy et al., 1996). Total loss of Ocn in rats resulted in bones with significantly increased trabecular thickness, density, and volume. Cortical bone volume and density were not increased in null animals (Lambert et al., 2016). These results were inconsistent with the theoretically predicted functions of Ocn and brought certain difficulties to identify the role of Ocn in bone. In the follow-up studies, the Karsenty team demonstrated that uncarboxylated osteocalcin (ucOcn) had effects on energy metabolism, male fertility, brain function as well as muscle function and proposed that ucOcn is a hormone secreted by bone (Lee et al., 2007; Oury et al., 2011; Oury et al., 2013; Mera et al., 2016).

On the contrary, two recent studies reported inconsistent conclusions. Moriishi et al. (2020) constructed a new Ocn<sup>-/-</sup> mouse model which was backcrossed to C57BL/6N more than 8 times before analysis, while the previous Ocn<sup>-/-</sup> mice published in 1996 were analyzed in the mixed background of C57BL/6J and 129/SV. The results suggested that ocn is necessary for aligning apatite crystallites but is not involved in regulating bone quantity by analysis of mice with deleted *Bglap* and *Bglap2* genes. Glucose metabolism, testosterone synthesis, and muscle mass are also normal in Ocn-deficient mice. Diegel CR finds alterations in the maturity of collagen and carbonate-to-phosphate ratio in cortical bone. Still, bone mass, serum glucose levels and male fertility were no different in the mice with a new *Bglap* and *Bglap2* double-knockout (dKO) allele compared with wild-type littermates (Diegel et al., 2020). The above results indicate that the role played by Ocn in the skeleton has not yet been fully elucidated. In addition, most of the existing research mainly used *Bglap* and *Bglap2* knockout mice, but the functional significance of the *Bglap3* allele in mice is also

unclear and the potential contributor of the *Bglap3* gene can not be ruled out.

With the development of technology, more methods could be used to assess bone microarchitecture and mineral composition. Conventional X-ray diffraction (XRD) can give direct information about the crystalline quality and size as well as the presence of defects in the crystal (Lai et al., 2016). In terms of evaluating bone mineralization, quantitative backscattered electron imaging (qBEI), quantitative magnetic resonance (QMR), micro-computed tomography ( $\mu$ CT), Fourier-Transform Infrared Spectroscopy (FTIR), and Raman spectroscopy analysis (RS) can be used to quantify the degree of bone mineralization and obtain bone microstructure data with different resolutions (Donnelly, 2011). Among these methods, FTIR and RS technology could provide the amount of minerals in each organic matrix unit by calculating the mineral-to-matrix ratio (MMR). The  $\mu$ CT process can determine the mineral density (mgHA/cm<sup>3</sup>) and bone microstructure (Paschalis et al., 2017). The  $\nu_1$ PO<sub>4</sub> and AmideI peaks of the RS test are sensitive to the detection of the incident angle, which can provide information on the alignment direction of hydroxyapatite crystals and collagen from a microscopic perspective. In addition, RS can scan different points separately to obtain the angular relationship between hydroxyapatite and collagen at various sites. These technological advances allow researchers worldwide to analyze Ocn biology in bone at unprecedented detail.

Using  $\mu$ CT, Bailey et al. (2017) found that Ocn and OPN work together to maintain the quality of bone materials, and Ocn knockout has a more significant impact than OPN. A computational study was presented to elucidate the critical roles of Ocn and OPN at the nanoscale interfibrillar interface and reveals the extremely high interfacial toughness of the Ocn/OPN (Wang et al., 2020). With the help of XRD and TEM, Iline-Vul et al. (2019) suggested that the post-translationally added  $\gamma$ -carboxylates Ocn has a marked regulatory effect on the mineral phases coating the apatite crystallites formed. The c-axis orientation of crystallography in Ocn knockout mice was poor consistency (tested by XRD technology), which means that Ocn deficiency may affect bone microstructure (Komori, 2020; Moriishi et al., 2020).

To elucidate the function of Ocn in bone more comprehensively, we generated Ocn<sup>-/-</sup> mice with simultaneous knockout of all three Ocn genes including *Bglap*, *Bglap2*, and *Bglap3*. Taking advantage of the property that the RS method is sensitive to the angle of hydroxyapatite and collagen we examined the correlation between hydroxyapatite and collagen micro alignment angle in the mouse femoral cortical bone area and acquired direct evidence of the effect of Ocn deficiency on bone mineral alignment. We applied FTIR and  $\mu$ CT to observe the effect of Ocn knockout on bone mass and quality, and Scanning electron microscopy (SEM) was used for imaging bone structure from the microscale to sub-cellular scales. Meanwhile, a tail-suspended mouse model was utilized to study the influence of Ocn on the stability of mineral components in the hindlimb unloading state. Our data showed that Ocn regulates the alignment of minerals parallel to collagen fibrils. This structural change further affects the ability of bone to maintain mineral stability, demonstrating that Ocn plays an essential role in bone structure maintenance.

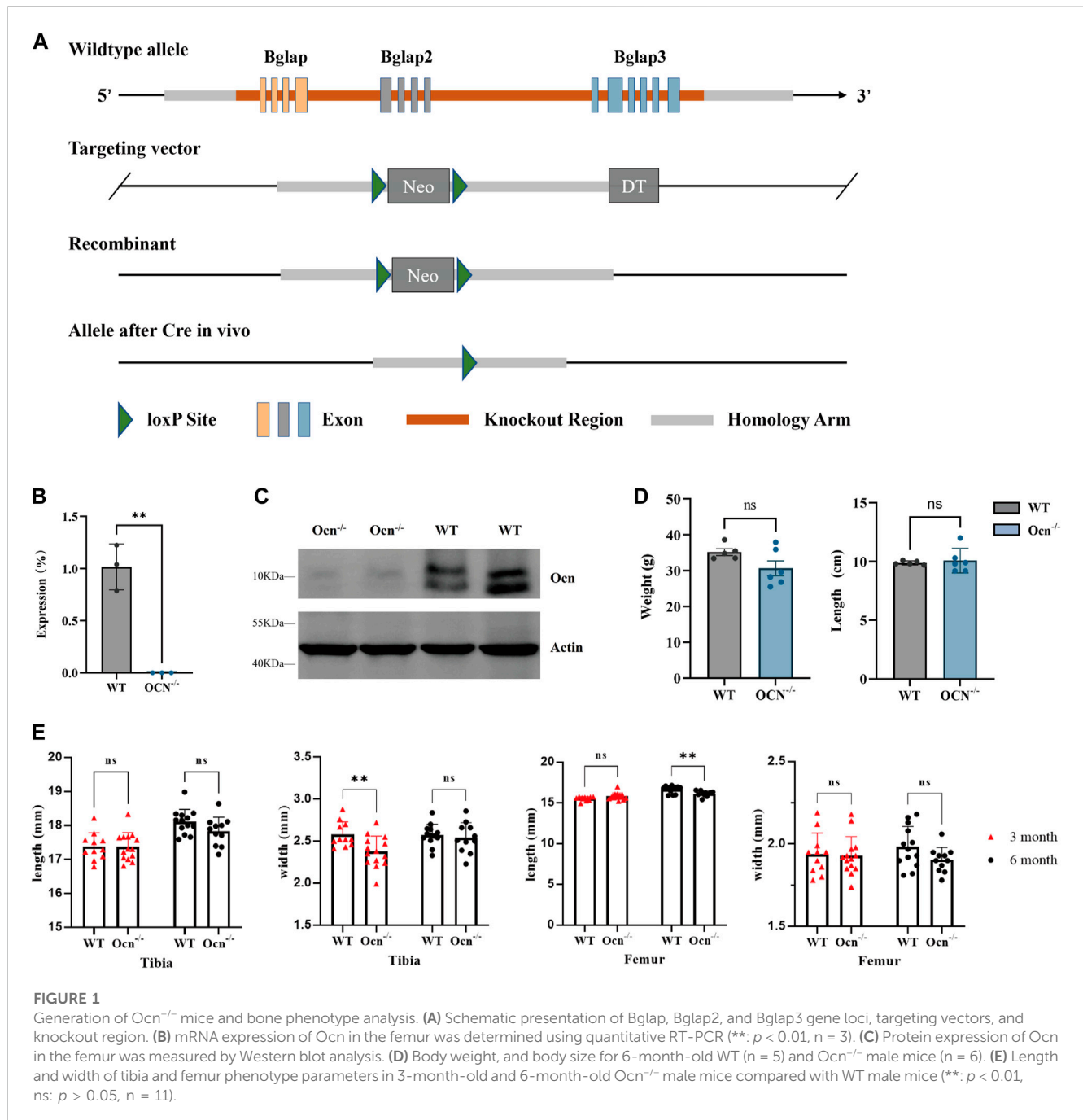


**FIGURE 1** Generation of *Ocn*<sup>-/-</sup> mice and bone phenotype analysis. **(A)** Schematic presentation of *Bglap*, *Bglap2*, and *Bglap3* gene loci, targeting vectors, and knockout region. **(B)** mRNA expression of *Ocn* in the femur was determined using quantitative RT-PCR (\*\*:  $p < 0.01$ ,  $n = 3$ ). **(C)** Protein expression of *Ocn* in the femur was measured by Western blot analysis. **(D)** Body weight, and body size for 6-month-old WT ( $n = 5$ ) and *Ocn*<sup>-/-</sup> male mice ( $n = 6$ ). **(E)** Length and width of tibia and femur phenotype parameters in 3-month-old and 6-month-old *Ocn*<sup>-/-</sup> male mice compared with WT male mice (\*\*:  $p < 0.01$ , ns:  $p > 0.05$ ,  $n = 11$ ).

## 2 Materials and methods

### 2.1 Animal experiments generation of *Ocn*<sup>-/-</sup> mice by homologous recombination method

*Ocn* KO mice, which possess a loxP site flanking *Bglap*, *Bglap2*, and *Bglap3* genes, were generated using the homologous recombination method (Cyagen Biosciences, Inc., Sunnyvale, CA). The targeting strategy allows the generation of conventional knockout mice with *Bglap*- *Bglap2*- *Bglap3* genes. Briefly, a homology region covering mouse *Bglap* to *Bglap3* was subcloned

into the targeting vector. One *Loxp* site was introduced into the *Bglap* promoter region, and another *Loxp* site together with a modified *Rox*-flanked *Neo* cassette was introduced into the region after *Bglap3* (Figure 1A). The 5'homology arm and 3'homology arm were amplified from BAC (RP24-171H19) DNA and confirmed by end sequencing. After linearization, the targeting vector was transfected into C57BL/6N background mouse embryonic stem cells. The positive clones were selected by G418 and injected into mouse blastocysts, which were then implanted into pseudo-pregnant females. F0 chimeric mice were further bred to C57BL/6N wild-type mice to generate F1 heterozygous mice. *Ocn*<sup>+/-</sup> mice were generated by crossing

Ocn<sup>fllox/fllox</sup> mice with CMV-Cre mice (B6.C-Tg (CMV-cre)1Cgn/J). Male and female heterozygous mice were crossed to generate homozygote Ocn<sup>-/-</sup> mice, and Wild-type control mice (WT) were derived from littermates. The expression of Ocn was analyzed by RT-PCR. All test items used male mice for experimentation. Before the study, all experiments were reviewed and approved by the Animal Care and Use Committee of China Astronaut Research and Training Center (No. ACC-IACUC-2021-032). Animals were housed in a specific-pathogen-free environment on a 12-h light cycle at 22°C ± 2°C temperature-controlled conditions. All the animals were supplied with food and water and were sacrificed by cervical dislocation at respective time points.

## 2.2 Real-time RT-PCR analysis and Western blot analysis

The total femur bone tissues were ground under liquid nitrogen and RNA was extracted by TRIzol (Invitrogen, Waltham, MA, United States), and then reverse transcription into cDNA was performed using a PrimeScript RT reagent kit (Takara, Dalian, China). Quantitative real-time PCR was performed using TB Green Premix Ex Taq II (Tli RNaseH Plus). The primer sequences of Ocn were designed to encompassing both of the three genes. Primers were designed using Primer 3. Ocn: Forward 5'-TGACAAAGCCTTCATGTCCA-3', Reverse 5'-TAGTGATACCATAGATGCGT-3'; Actin: Forward 5'-TCA GATGAATTTTCGTTGGCAGA-3', Reverse 5'-GAGCACTTG GGTACTCCACG-3'. We used WT and KO primers to identify wild-type and Ocn knockout mice, respectively. Mice with both primer bands were heterozygous. WT: Forward 5'-ATGAGGGAGACAACAGGGAGGAA-3', Reverse 5'-TTTGCT GATTTGTGTGTTGGATGT-3'; KO: Forward 5'-AGCATCCTT TGGGTTTGAC-3', Reverse 5'-AGGGAGGCATTCTGTG TG-3'.

For Western blot analysis, The total femur bone tissues were ground under liquid nitrogen and then lysed by RIPA buffer containing protease inhibitor cocktail (Roche, German). The membrane was blocked with 5% BSA in Tris-buffered saline containing 0.1% Tween 20 (TBST) for 1 h and then incubated overnight. For the detection of osteocalcin, we used anti-osteocalcin Ab (Affinity Biosciences, Cincinnati, OH, United States) and anti-Actin Ab (Servicebio, Wuhan, China). Signals were detected using enhanced luminescence (Bio-Rad, United States).

## 2.3 Raman spectroscopy analysis (RS)

Femurs were harvested from 6-month-old mice (Ocn<sup>-/-</sup> and WT mice). Specimens were processed for cold polymethyl methacrylate (PMMA) embedding. Subsequently, the femur was sliced transversely into 10 µm cross sections at position 7 (Figure 4A), and the rest of the femur was sliced into 10 µm longitudinal sections. Selected points evenly distributed throughout the sectioned tissue from each bone cross-section were analyzed by Raman spectroscopy (Renishaw in *via*, Wotton-under-Edge, Gloucestershire, United Kingdom). The test points on the longitudinal section

were at position 7, and each of the upper and lower cortical bone sections has two points side by side. A 785 nm laser was used to excite the electrons within the material, and 50× objective and the numerical aperture of 0.75 produced a laser spot of approximately 2 µm in diameter. The acquisitions were made in the spectral range of 100 cm<sup>-1</sup>–3500 cm<sup>-1</sup>, with an integration time of 30 s and one accumulation. Three spectra were acquired for each point, and 4 points were measured for every 24 samples. Normalization and baseline subtraction was performed on all ranges to obtain a pure bone tissue Raman spectrum signal. Raman spectrum showing the assignments for ν<sub>1</sub>PO<sub>4</sub> (961–962 cm<sup>-1</sup>), ν<sub>2</sub>PO<sub>4</sub> (430–431 cm<sup>-1</sup>), Amide I (1667–1670 cm<sup>-1</sup>), Amide III (1248–1252 cm<sup>-1</sup>), Proline (855–858 cm<sup>-1</sup>).

## 2.4 Scanning electron microscopy analysis (SEM)

Scanning electron microscopy analysis of mice femur sections was performed on a Hitachi S4800 high-resolution field-emission scanning electron microscopy with an accelerating voltage of 3.0 kV. Secondary electrons were obtained using a through-lens detector and were recorded at a 7.6 mm and 8.0 mm working distance. ImageJ software was used to analyze the gap area proportion of the transverse cross-section at position 7.

## 2.5 Fourier transform infrared spectroscopy (FTIR)

Femurs were harvested from 6-month-old mice (Ocn<sup>-/-</sup> and WT mice) and then embedded with cold polymethyl methacrylate (PMMA). The samples were sliced transversely into 10 µm cross sections at position 7 and position 9 (Figure 4A). For FTIR analysis, Six selected points were randomly distributed throughout the sectioned tissue analysis (Nicolet iN10, Thermo Scientific, Waltham, MA, United States). Prior to analysis, the scanning range was set to 450–7,600 cm<sup>-1</sup> with a spectral resolution of 4 cm<sup>-1</sup>. Signals were acquired every 2 min, and the field of view was 100 µm<sup>2</sup> (10 µm\*10 µm). The indexes were calculated by the following: mineralization = mineral (916–1180)/matrix (1588–1712); carbonate/matrix = carbonate (840–890)/matrix (1588–1712); carbonate/mineral = carbonate (840–890)/mineral (916–1180); collagen maturity = 1667/1685; crystallinity = 1030/1020; carbonate substitution = TypeA (878–879), TypeB (871–893), TypeL (865–867); HPO<sub>4</sub>/mineral = 1106/961, 1075/961, 1145/mineral (Courtland et al., 2008).

## 2.6 Micro CT (µCT)

The skin was removed from the mouse femurs and they were fixed in 70% ethanol. The whole secondary spongiosa of the left distal femur from each mouse was scanned *ex vivo* using a micro CT system (mCT40, SCANCO MEDICAL, Switzerland). The micro CT analysis followed the ASBMR standards (Bouxsein et al., 2010). The micro CT scan acquisition parameters were: voxel size = 39 µm<sup>3</sup>, X-ray energy = 70 keV, X-ray tube = 70 kVp, X-ray intensity =

114  $\mu\text{A}$ , integration time = 200 ms. A total of 850 slices with a voxel size of 10.5  $\mu\text{m}$  were scanned in the distal femur. Eighty slices of cortical and trabecular bone at position 9 (proximal to the distal growth plate) and eighty slices of cortical bone at position 7 (2.5 mm from the growth plate) were selected for analysis. The parameters cortical thickness (Ct.Th), bone volume fraction (BV/TV), trabecular number (Tb.N), trabecular thickness (Tb.Th) and trabecular separation (Tb.Sp) were calculated from the three-dimensional reconstruction of the selected slices.

## 2.7 Tail suspension experiment

The Tail suspension manipulation was performed as Wronski described previously (Wronski and Morey-Holton, 1987) with minor modifications as we used before (Zhang et al., 2020). Six-month-old male mice were suspended by the tail attached to a chain hanging from a beam using a strip of adhesive surgical tape and maintained one per cage while they were tail-suspended. The bodies of mice were at a 30° angle to the floor, with only the forelimbs touching the floor and allowed to freely move to food and water. The mice were sacrificed by rapid cervical dislocation after hindlimb unloading for 28 days. FTIR and  $\mu\text{CT}$  were used to analyze bone minerals and microstructure before and after tail suspension in Different cohorts of mice.

## 2.8 Data analyze

Indexes statistical analyses were performed using the Student's *t*-test to compare WT and  $\text{Ocn}^{-/-}$  or using two-way ANOVA to compare WT and  $\text{Ocn}^{-/-}$  and their tail-suspended test groups in  $\mu\text{CT}$  analysis by Prism 9.0 (GraphPad Prism software). Data were presented as mean  $\pm$  standard deviation (SD). The Raman spectroscopy regression models were built using the Huber-loss function (Huber Regressor) with python v3.7 (Python Software Foundation). Statistical in RS was analyzed by comparing the  $\Delta y$  value (distance value  $y$  from each point to the fitted curve) between the two genotype groups using a *t*-test. For FTIR in Figure 5, the data was displayed in the form of the percentage change. Percentage (%) was calculated by dividing each value by the average value of the WT control group.

# 3 Results

## 3.1 Physiological measurements of femur phenotype in $\text{Ocn}^{-/-}$ mice

To generate *Bglap*, *Bglap2*, and *Bglap3* triple-knockout mice, genomic DNA encompassing all three genes was replaced with the neo gene (Figure 1A). Real-time RT-PCR analysis indicated that the expression of *Ocn* was absent in  $\text{Ocn}^{-/-}$  mice using an *Ocn* triple-gene consensus segment primer (Figure 1B; Supplementary Figure S1). The expression of proteins was assessed by Western blotting, and *Ocn* proteins were also absent in  $\text{Ocn}^{-/-}$  mice (Figure 1C). There were no significant differences in body weight and body length between WT and  $\text{Ocn}^{-/-}$  male mice (Figure 1D). We then measured

the bone phenotype of the Tibia and Femur in 3-month and 6-month-old mice. The Tibia width significantly decreased in 3-month-old  $\text{Ocn}^{-/-}$  mice. However, there was no intergroup difference between 6-month-old  $\text{Ocn}^{-/-}$  and WT mice. The Femur length significantly decreased in 6-month-old  $\text{Ocn}^{-/-}$  mice. No significant differences were observed between the other comparison groups (Figure 1E).

## 3.2 *Ocn* deficiency results in the disordered alignment of collagen fibers and hydroxyapatite crystals in bone

Raman spectroscopy (RS) can be used as a complementary tool for bone diagnosis due to its ability to assess compositional and organizational characteristics of both collagen and mineral. As described in the calculation method section, the ratio of organic and inorganic peaks was compared, and linear fitting was performed to judge the changes of collagen and hydroxyapatite arrangement angle in bone (Figure 2A). Three types of calculations for mineral/matrix ratios can be described as follows: mineral/matrix A = ( $\nu_1\text{PO}_4/\text{AmideI}$ )  $\gamma$  (where  $\gamma$  is angle coefficient), mineral/matrix B = ( $\nu_2\text{PO}_4/\text{AmideIII}$ ), mineral/matrix C = ( $\nu_1\text{PO}_4/\text{Proline}$ ) (Makowski et al., 2013). The ratio of  $\nu_1\text{PO}_4/\text{AmideI}$  ratio varied upon changing the measurement angles of the RS analysis. When the angle between hydroxyapatite crystals and collagen is uncertain,  $\gamma$  cannot be calculated, and the accurate mineral matrix ratio through  $\nu_1\text{PO}_4/\text{AmideI}$  can not be drawn. However, the ratio of  $\nu_1\text{PO}_4/\text{Proline}$  or  $\nu_2\text{PO}_4/\text{AmideIII}$  are angle-insensitive, and mineral/matrix B and mineral/matrix C can accurately describe the mineral matrix ratio. In that case, every test point of mineral/matrix B and mineral/matrix C had an excellent linear fitting, but mineral/matrix A could not. Therefore, the linear fit between each of the two ratios could be used to calculate whether the alignment between hydroxyapatite crystals and collagen is consistent.

We calculated the three ratios in the bone longitudinal section and transverse cross-section and performed a linear fit between any two ratios using the Huber loss function (Huber Regressor). The results revealed a high fit of  $\nu_1\text{PO}_4/\text{Proline}$  and  $\nu_2\text{PO}_4/\text{AmideIII}$  groups in both WT and  $\text{Ocn}^{-/-}$  male mice as expected (Figure 2B). Impressively, the  $R^2$  (goodness-of-fit measure for linear regression models) of the linear regression model of  $\nu_2\text{PO}_4/\text{AmideIII}$  and  $\nu_1\text{PO}_4/\text{AmideI}$  was much lower in  $\text{Ocn}^{-/-}$  mice than in WT mice (Figure 2C). The  $R^2$  of the linear regression model of the  $\nu_1\text{PO}_4/\text{Proline}$  and  $\nu_1\text{PO}_4/\text{AmideI}$  was also lower in  $\text{Ocn}^{-/-}$  mice (Figure 2D). These results suggested that the alignment of collagen fibers and hydroxyapatite crystals was disordered in  $\text{Ocn}^{-/-}$  mice.

## 3.3 SEM images analyzed showed a significant increase in gap area in the $\text{ocn}^{-/-}$ mice

A commonly used technique for imaging bone structure from microscale to sub-cellular scales is scanning electron microscopy (SEM). The standard SEM can provide high-resolution images on the order of a few nm (2–10 nm) (Ambekar et al., 2012). To investigate the effects of collagen arrangement on the bone structure, we used SEM to analyze the femur longitudinal section

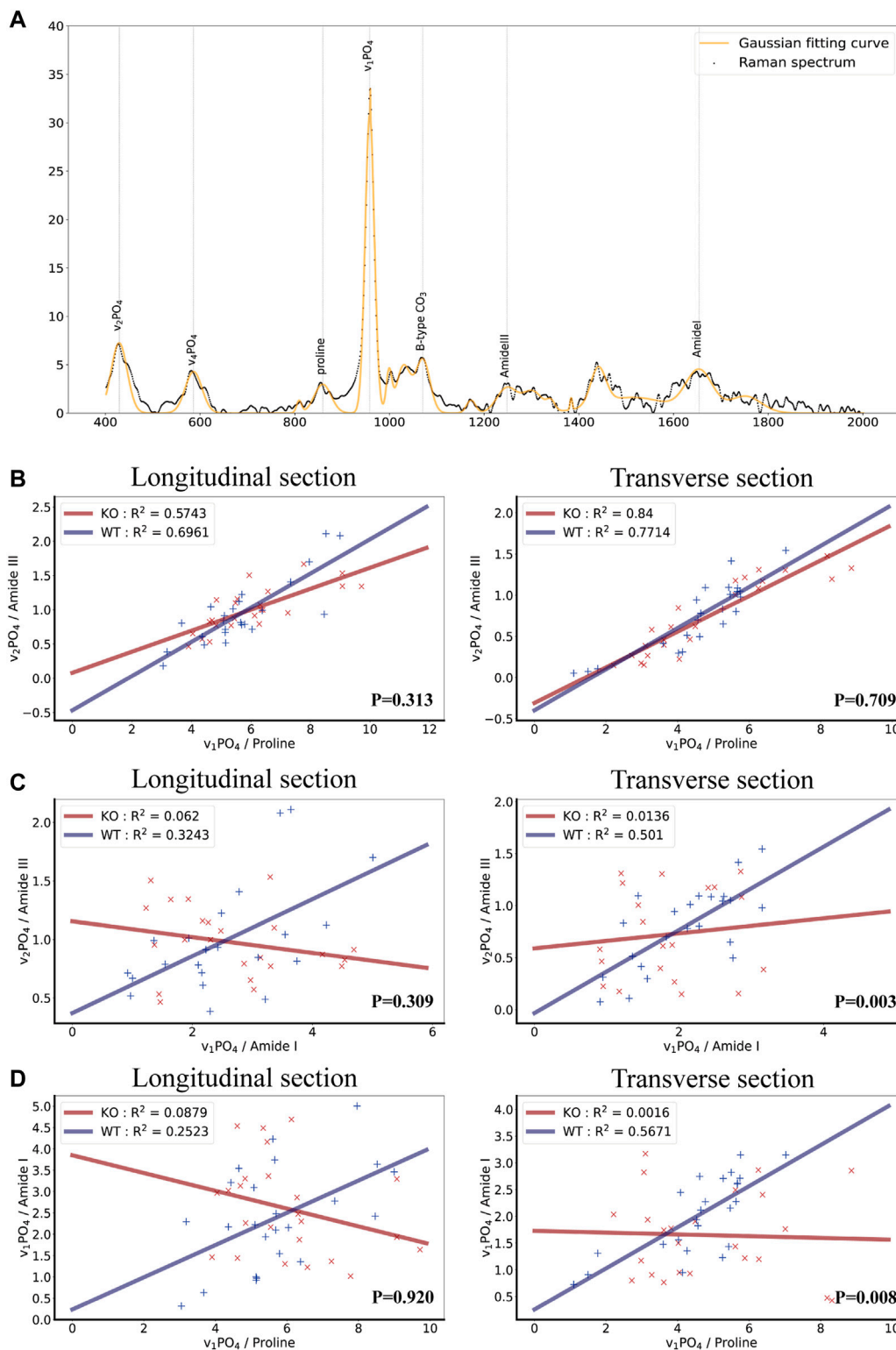
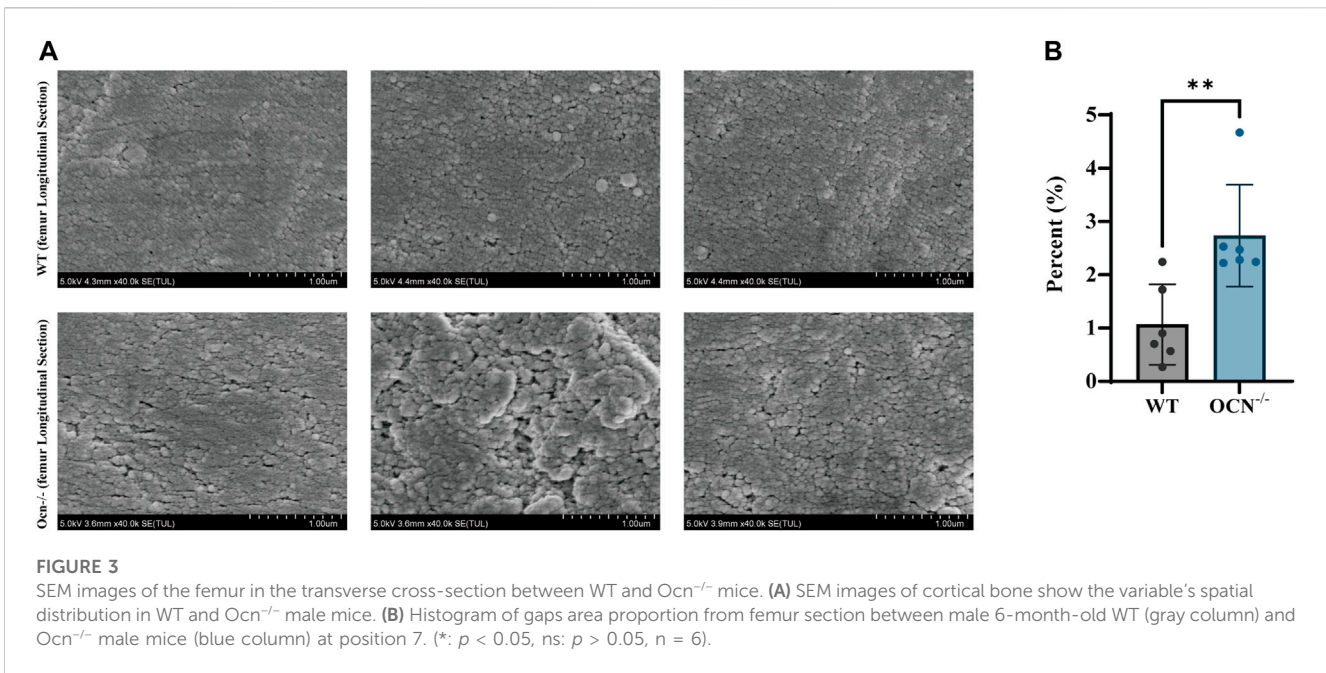


**FIGURE 2**

Biochemical properties of bone as measured by Raman spectroscopy in wild-type and *Ocn*<sup>-/-</sup> mice. **(A)** Raman spectrum and Gaussian fitting curve of bone tissue showing the major bands and the corresponding compounds. The background signal has been removed. **(B)** Scatter plots, fitted lines, and correlation coefficient ( $R^2$ ) of  $\nu_1\text{PO}_4/\text{Proline}$  and  $\nu_2\text{PO}_4/\text{Amide III}$  groups in both WT and *Ocn*<sup>-/-</sup> (KO) male mice (Left: longitudinal section, Right: Transverse section,  $n = 6$ ). **(C)** Corresponding analysis of  $\nu_2\text{PO}_4/\text{Amide III}$  and  $\nu_1\text{PO}_4/\text{Amide I}$  groups in both WT and *Ocn*<sup>-/-</sup> (KO) male mice (Left: longitudinal section, Right: Transverse section,  $n = 6$ ). **(D)** Corresponding analysis of  $\nu_1\text{PO}_4/\text{Proline}$  and  $\nu_1\text{PO}_4/\text{Amide I}$  groups in both WT and *Ocn*<sup>-/-</sup> (KO) male mice (Left: longitudinal section, Right: Transverse section,  $n = 6$ ). (P: comparing the  $\Delta y$  value (distance value  $y$  from each point to the fitted curve) between the two genotype groups using a  $t$ -test).



morphology in a position consistent with the RS scan. As shown in **Figure 3A**, a looser surface structure of bone particles was observed in the *Ocn*<sup>-/-</sup> male mice compared with WT male mice. We also counted the area and perimeter of the gaps between particles (**Supplementary Figure S2**). There was a significant increase in gap area proportion in the *Ocn*<sup>-/-</sup> mice, indicating a large and irregular gap between the femoral microstructures (**Figure 3B**).

### 3.4 Fourier transform infrared spectroscopy (FTIR) analysis showed few differences in bone mineral index between WT and *ocn*<sup>-/-</sup> mice

The chemical aspects of the bone matrix were analyzed in the posterior part of the femurs (Position 7 and Position 9) by FTIR (**Figure 4A**). Seven indexes including mineralization, carbonate/matrix, carbonate/mineral, collagen maturity, crystallinity, carbonate substitution (3 algorithms: typeA, typeB, typeL), and HPO<sub>4</sub>/mineral were used for assessing the constitution of the bone matrix between WT and *Ocn*<sup>-/-</sup> male mice in bone sections (**Faibish et al., 2005; Courtland et al., 2008**). There was a significant decrease ( $p < 0.05$ ) in mineral/matrix at position 7 and a significant increase ( $p < 0.05$ ) in crystallinity at position 9 in the *Ocn*<sup>-/-</sup> mice compared with WT mice. No significant differences were found in other indexes between the two groups (**Figures 4B, C**).

### 3.5 The bone mineral content changed more variable in *ocn*<sup>-/-</sup> mice than in WT mice under the tail suspension test

The tail suspension was performed to achieve an unloading status of hindlimbs (**Cryan et al., 2005**). This animal model can be

used to analyze the effect of *Ocn* deficiency on bone during unloading. After 28 days of the tail-suspension test, FTIR parameters of femur microarchitecture were measured using the previously described methods in WT and *Ocn*<sup>-/-</sup> male mice. Except for mineralization value in WT mice, we found no significant difference in other FTIR indexes at position 7 during the experiment (**Figure 5A**). However, mineralization, carbonate/matrix, collagen maturity, and crystallinity significantly decreased ( $p < 0.05$ ) in *Ocn*<sup>-/-</sup> mice compared with WT mice. These results indicated that *Ocn* deficiency accelerates mineral loss. Regarding crystal replacement, carbonate substitution was significantly decreased at position 9 in the *Ocn*<sup>-/-</sup> mice. Meanwhile, each index of HPO<sub>4</sub>/mineral significantly increased, and this change was less pronounced in WT mice (**Figure 5B**). Therefore, the inconsistent arrangement of hydroxyapatite and collagen may decrease hydroxyapatite stability, and *Ocn* knockout mice were more likely to have crystal replacement during bone loss.

### 3.6 Effect of *Ocn* knockout on the bone microstructure caused by the tail suspension

To examine the effect of *Ocn* knockout-mediated alteration of microstructural morphology in bone, we used  $\mu$ CT scanning to quantify the changes in the bone microstructure of the WT and *Ocn*<sup>-/-</sup> male mice and their tail-suspended test groups (**Figures 6A–C**). We analyzed the thickness of cortical (Ct.Th) of cortical regions at position 7 and position 9, and BV/TV, trabecular (Tb.N), thickness (Tb.Th) and separation (Tb.Sp) of trabecular regions at position 9. The scanning results demonstrated that these indexes have no significant difference between WT and *Ocn*<sup>-/-</sup> mice before the tail suspension (**Figures 6D, F**). After 28 days of tail suspension, the cortical bone thickness at position 7 and 9 decreased significantly (**Figure 6D**), and the reduction ratio was greater in *Ocn*<sup>-/-</sup> mice than

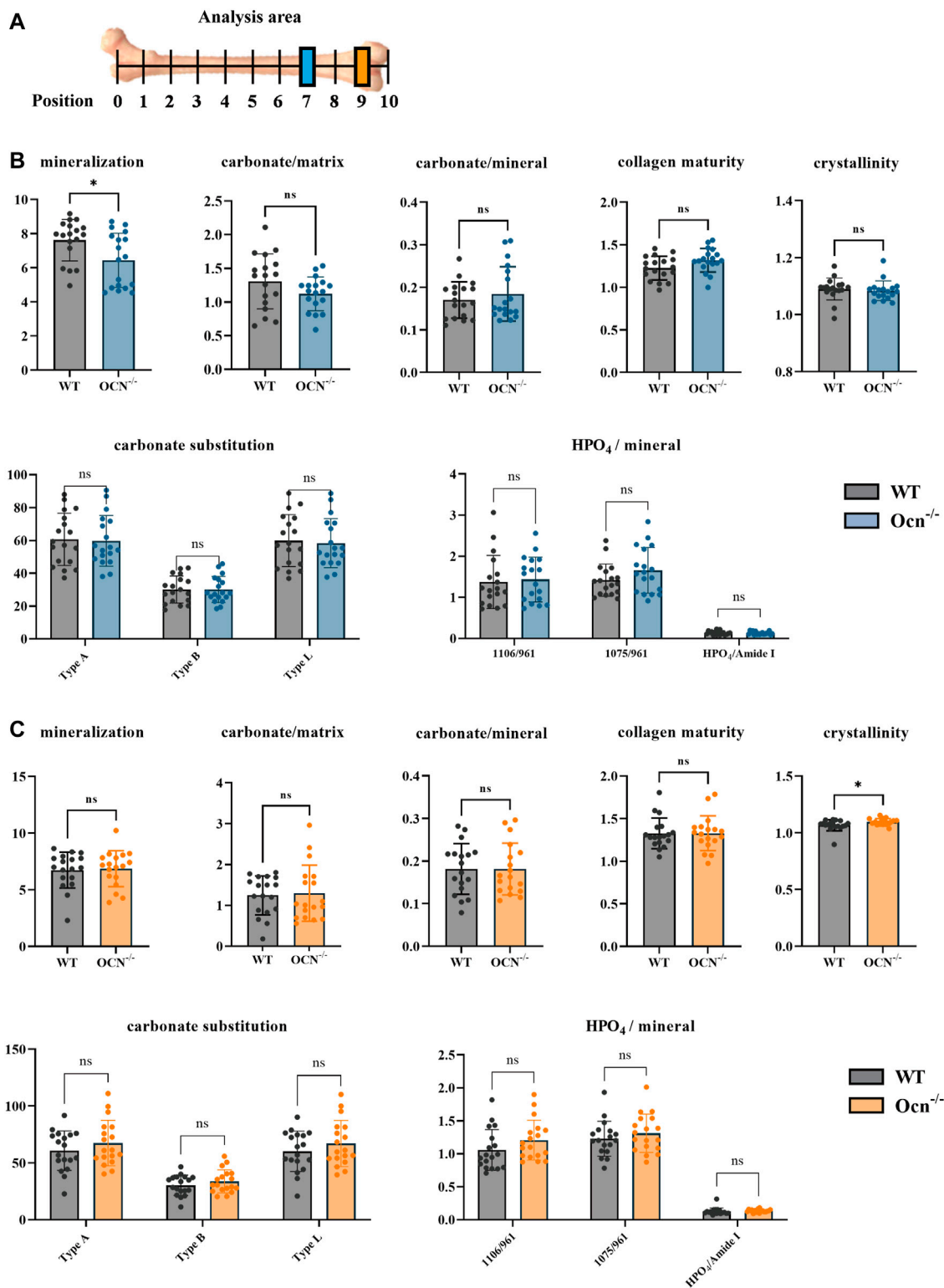
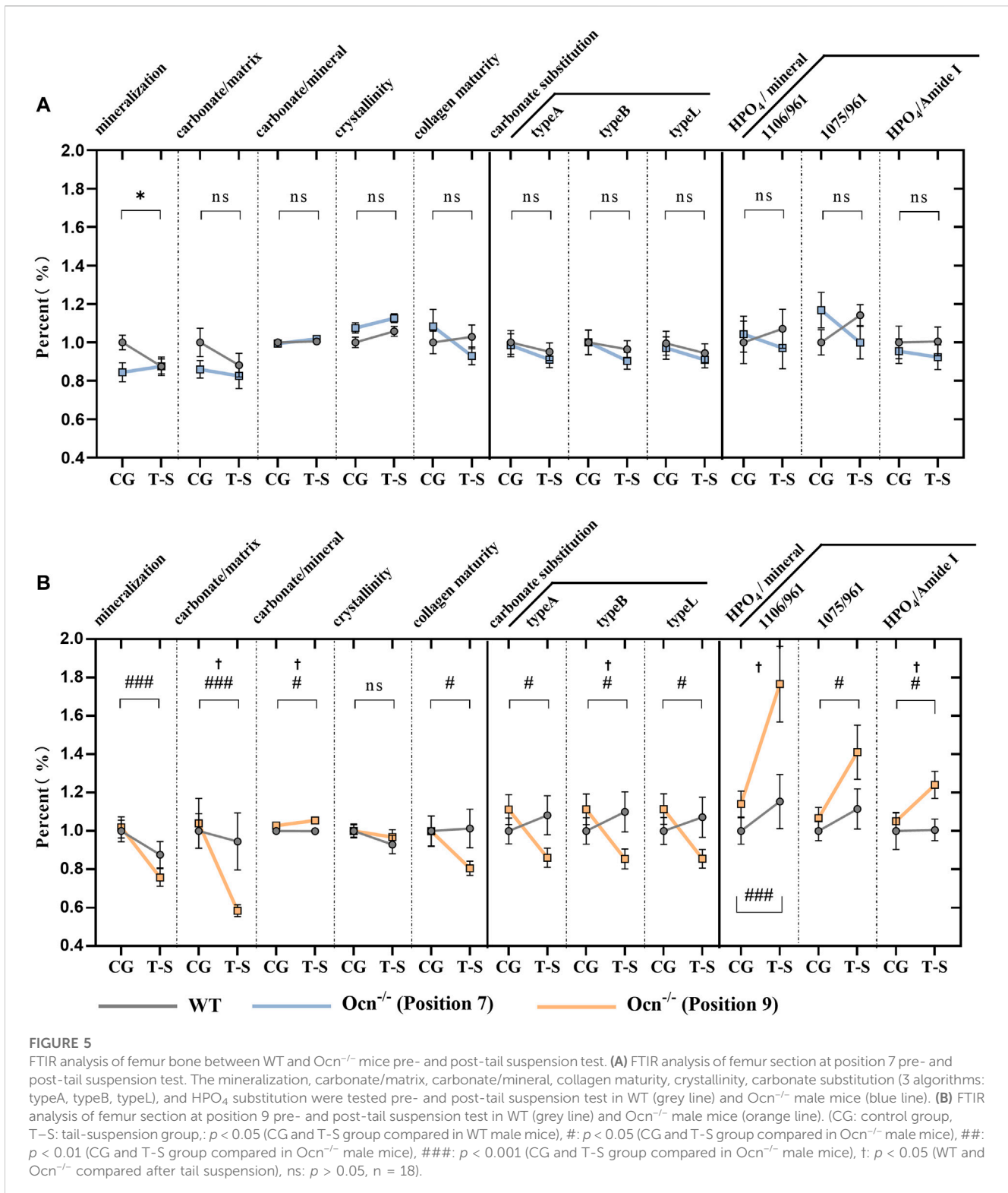


**FIGURE 4**

An FTIR analysis showed few differences in bone mineral index between WT and *Ocn*<sup>-/-</sup> mice. **(A)** Schematic presentation of analyzed positions of bone section used for FTIR (Color annotation for Position 7 (WT: grey, *Ocn*<sup>-/-</sup>: blue) and Position 9 (WT: grey, *Ocn*<sup>-/-</sup>: orange)). **(B)** FTIR analysis of position 7 femur section at 6 months of age. The mineralization, carbonate/matrix, carbonate/mineral, collagen maturity, crystallinity, carbonate substitution (3 algorithms: typeA, typeB, typeL), and HPO<sub>4</sub>/mineral were compared between WT and *Ocn*<sup>-/-</sup> mice. **(C)** FTIR analysis of position 9 femur section at 6 months of age. The analysis indexes were the same as the detection indexes in position 9 compared between WT mice and *Ocn*<sup>-/-</sup> male mice. (\*: *p* < 0.05, ns: *p* > 0.05, *n* = 18).



in WT mice at position 9 (Supplementary Figure S3A, B). The trabecular regions at position 9 showed significant bone loss after tail suspension, with BV/TV and Tb.Th decreased significantly, and Tb.N and Tb. Sp increased significantly (Figures 6E, F). However, there was no significant difference in the trabecular bone between the two groups of tail-suspended mice (Supplementary Figure S3C).

## 4 Discussion

In this study, we generated triple-gene knockout mice for *Bglap*, *Bglap2*, and *Bglap3*, which encode osteocalcin (*Ocn*). This is the first study to examine the effects of deleting all three *Ocn* genes in mice with a C57BL/6J genetic background. Our findings could

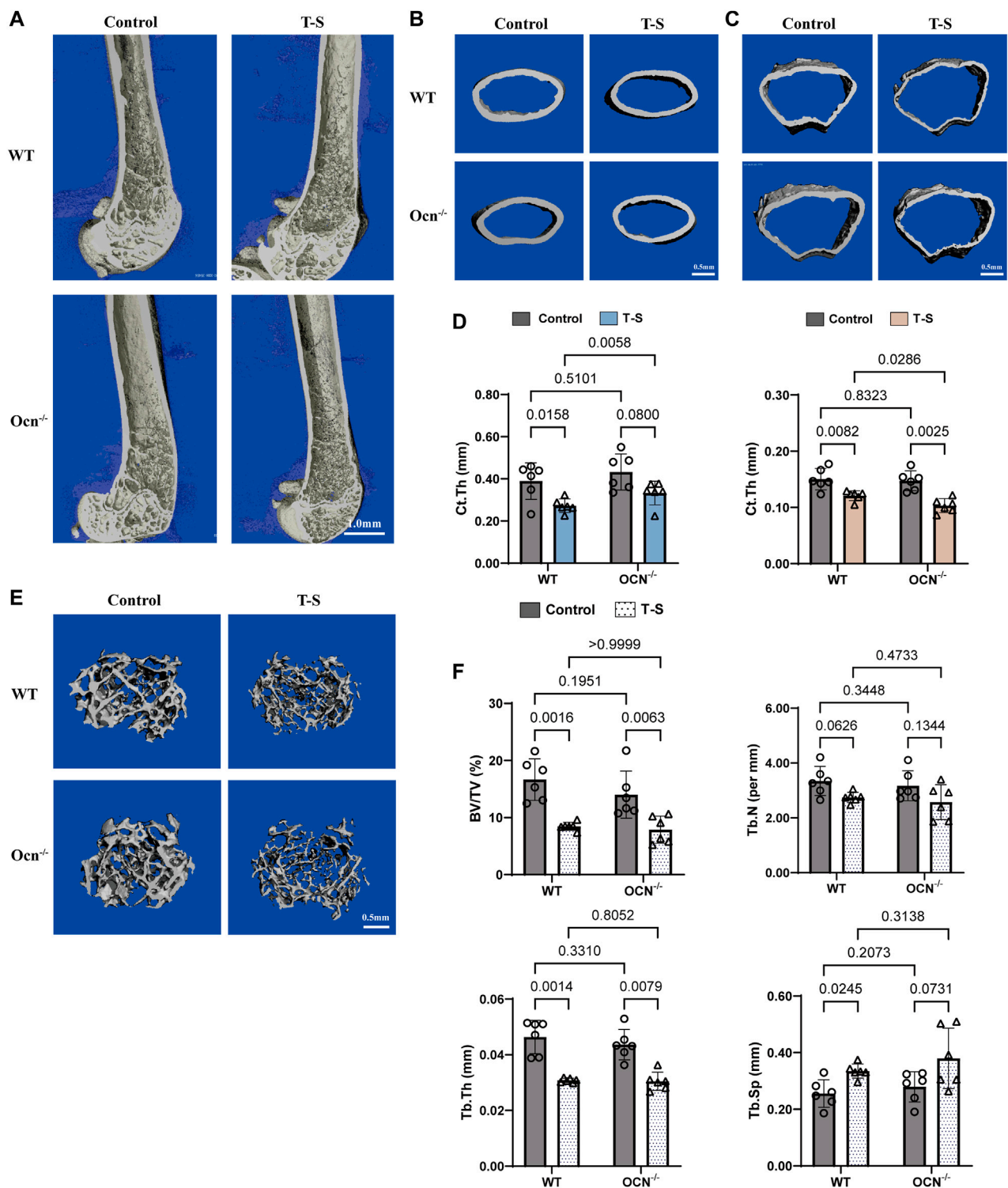


**FIGURE 6**  $\mu$ CT analysis of femur bone before and after tail suspension test. (A–C) Representative 3D  $\mu$ -CT images of distal femur and cortical regions from 6-month-old WT and  $Ocn^{-/-}$  male mice (Scale bars: 1 mm for the femur and 0.5 mm for cortical regions). (D)  $\mu$ CT analysis of Ct.Th in cortical regions at position 7 and position 9 from WT and  $Ocn^{-/-}$  mice before and after tail suspension test (Control: control group, T-S: tail-suspension group, n = 6). (E) Representative 3D  $\mu$ -CT images of trabecular regions from 6-month-old WT and  $Ocn^{-/-}$  male mice (Scale bars: 0.5 mm). (F)  $\mu$ CT analysis of BV/TV, Tb.N, Tb.Sp and Tb.Th in trabecular regions at position 9 from WT and  $Ocn^{-/-}$  mice before and after tail suspension test (Control: control group, T-S: tail-suspension group, n = 6).

complement previous studies using different *Ocn* knockout models. We measured bone mass and quality at two different sites of the femur using RS, SEM, FTIR, and  $\mu$ CT methods. We observed that the alignment of collagen fibers and hydroxyapatite crystals was disrupted in *Ocn*<sup>-/-</sup> mice by RS analysis. The gap area proportion was significantly increased in *Ocn*<sup>-/-</sup> mice, indicating large and irregular spaces between the femoral microstructures. The FTIR analysis showed that bone mineral index was similar between *Ocn*<sup>-/-</sup> mice and wild-type (WT) mice. However, *Ocn* deficiency caused the misalignment of collagen fibers and hydroxyapatite crystals in bone. Mineral loss was more rapid in *Ocn*<sup>-/-</sup> mice than in WT mice during tail suspension. The  $\mu$ CT scanning revealed that bone microstructure was comparable between WT and *Ocn*<sup>-/-</sup> mice before tail suspension. After 28 days of tail suspension, the cortical bone thickness decreased more in *Ocn*<sup>-/-</sup> mice than in WT mice at position 9. Taken together, these results suggest that *Ocn* regulates the organization of collagen fibers and hydroxyapatite crystals in bone.

Investigators have tried a variety of knockout mouse models to illuminate the function of *Ocn*. The first *Ocn*-deficient mice (*osc*<sup>m1</sup>/*osc*<sup>m1</sup>) were generated by simultaneously deleting both *Bglap* and *Bglap2* using embryonic stem cell technology (Ducy et al., 1996). The *Bglap3* gene was not deleted in this mouse model because the *Bglap3* is expressed in the kidney but not in bone (Rho et al., 1998). With this model, the researchers investigated the function of *Ocn* in bone and then demonstrated the endocrine regulation role of *Ocn* in regulating whole-body physiology, such as energy metabolism, male fertility, and brain development (Lee et al., 2007; Oury et al., 2011; Oury et al., 2013; Mera et al., 2016; Zoch et al., 2016; Khirmian et al., 2017; Yadav et al., 2022). Due to the essential functions of *Ocn*, another *Ocn*<sup>-/-</sup> mouse model was constructed with C57BL/6N genetic background. The only difference between the two mouse lines is that the previous *Ocn*<sup>-/-</sup> mouse model was generated in the mixed background of C57BL/6J and 129/SV (Moriishi et al., 2020). Meanwhile, Diegel et al. generated *Bglap/2*<sup>dko/dko</sup> by simultaneously injecting Cas9 protein and guide RNAs that recognize sequences within *Bglap* and *Bglap2* but not within *Bglap3* (Diegel et al., 2020). Although researchers broadly suggest that *Bglap3* may have low expression in bone, it remains to be determined if there are any compensatory mechanisms when *Bglap* and *Bglap2* gene is knockout. The functional significance of the *Bglap3* allele in mice is also unclear. Therefore, we constructed an *Ocn* triple-gene knockout mice to complement the *Ocn* function study.

*Ocn* promotes normal bone mineralization by regulating the growth of hydroxyapatite crystals (Hooshmand and Arjmandi, 2009). Tsao et al. (2017) investigate the roles of *Ocn* in mineral species production during the osteogenesis of MSCs. Using Raman spectroscopy, they found that the maturation of mineral species was affected by the *Ocn* expression level. The mineral species maturation was delayed, and total hydroxyapatite was lower in the *Ocn* knockdown group than in the control group. The *Ocn*-derived peptide, particularly in amidic form, can act as a bioactive inducer of the mineralization process, hence accelerating bone tissue regeneration (Hosseini et al., 2019). These studies indicate that *Ocn* may play a role in maintaining bone mass. However, the absence of *Ocn* leads to an increase in bone formation without impairing bone resorption (Ducy et al., 1996). Using an *Ocn*<sup>-/-</sup> rat model constructed by CRISPR/Cas9 technology, Lambert et al. (2016) found that complete loss of *Ocn* in the rat affected bone structure and

function, with increased trabecular bone and increased bone strength. Thus, these contradictory results cast doubt on the role of *Ocn* as one of the main factors in bone mass.  $\mu$ CT and 3-point bending tests do not find differences in *Bglap/2*<sup>dko/dko</sup> mice from wild-type littermates for bone mass and strength (Diegel et al., 2020), and *Ocn* is not involved in the regulation of bone quantity in *Ocn*-deficient mice (Moriishi et al., 2020). Our study investigates the function of *Ocn* in bone mass by  $\mu$ CT and found that bone mass was unchanged in the trabecular region after osteocalcin knockout. Until now, the study results remain conflicting, and further studies are warranted to confirm and explain the results.

The bone mineral is amorphous calcium phosphate (65% in young bone and 35% in adult bone), which is a precursor to crystalline hydroxyapatite (HAp), and fibrillar type I collagen provides a stable template for mineralization. Cross-linking is crucial for the stability and mineralization of collagen (Hakimimehr et al., 2005; Prabhakaran et al., 2009; Terajima et al., 2014). Thus, the proper amount and structure of the two matters play an essential role in bone formation and strength. Using small angle x-ray scattering (SAXS) and wavelength dispersive spectroscopy (WDS) on *OC*<sup>-/-</sup> (*Ocn*<sup>-/-</sup>) genetic knockout mice bones, Poundarik et al. (2018) demonstrated that *Ocn* has specific roles in the biomolecular regulation of minerals in bone. *Ocn* is localized to both intrafibrillar and interfibrillar collagen. In the former, *Ocn* binds to type I collagen and may mediate nucleation, growth, and development of platelet-shaped apatite crystals within structural units of collagen such as microfibrils, fibrils and fibers (Chen et al., 2015). Another study suggested that *Ocn* was not necessary for the regulation of bone formation or resorption but essential for the alignment of the BAp c-axis parallel to collagen fibrils and required for optimal bone strength (Moriishi et al., 2020). These studies indicated that *Ocn* plays an essential role in mineral and collagen fibril arrangement. By using FTIR and RS methods, we found that the alignment of collagen fibers and hydroxyapatite crystals was more disordered in *Ocn*<sup>-/-</sup> mice than in WT mice. Because of these structural features of binding calcium ions and hydroxyapatite, *Ocn* may have played a role in stabilizing the alignment of minerals and collagen in bone.

The tail-suspension mouse model is universally used to study unloading osteoporosis (Li et al., 2021; Camy et al., 2022; Zlotnick et al., 2022). We use the model to investigate the absence of *Ocn* on bone mass and bone minerals in the condition of bone loss. In the tail-suspended condition, *Ocn* knockout mice had a faster rate of mineral loss, and the proportion of carbonate substitution in the bone was also significantly reduced. Taken together, the loss of *Ocn* causes a disordered arrangement (low congruence) of collagen fibers and hydroxyapatite crystals, reducing the ability of the bone tissue itself to resist unloaded bone loss. In addition, we found that the No. 9 position of the femur of *Ocn*<sup>-/-</sup> mice was more prone to acid phosphate substitution after tail suspension. It is important to note that male mice were mainly used in this study. Female *Ocn* knockout mice on a B6 background had a lower bone mineral density, and lower mineral-to-matrix ratio resulting in reduced stiffness and weaker bone strength. Suggest that reduced *Ocn* may contribute to fracture and weaker bone in some groups of elderly and adults (Berezovska et al., 2019). Moriishi et al. (2020) and Diegel et al. (2020) used both male and female *Ocn* knockout mice and found that the alignment of apatite crystallites, but not endocrine abnormalities, or muscle mass was changed in *Ocn* knockout mice (Manolagas, 2020; Moriishi and

Komori, 2020). Taking into account the possible impact of gender, relevant research will be carried out in the future to explore the significance of this experimental result.

In conclusion, the alignment of hydroxyapatite crystals and collagen fibers showed inconsistency in *Ocn<sup>-/-</sup>* mice. The disordered arrangement of hydroxyapatite will lead to changes in bone mineral composition in the case of tail suspension simulating bone loss.

## Data availability statement

The raw data supporting the conclusion of this article will be made available by the authors, without undue reservation.

## Ethics statement

The animal study was reviewed and approved by ACC-IACUC-2021-032.

## Author contributions

Conceptualization: ZX, CY, ZD, and YL. Data curation: ZX, CY, FW, XT, ZD, and YL. Formal analysis: ZX, CY, FW, XT, HZ, HW, YG, ZX, MZ, SJ, ZD, and YL. Funding acquisition: CY, ZD, and YL. Investigation: FW, XT, HZ, HW, YG, XS, MZ, and SJ. Methodology: ZX, CY, FW, XT, HZ, HW, ZD, and YL. Project administration: ZX, CY, ZD, and YL. Resources: CY, ZD, and YL. Validation: ZX, CY, FW, and ZD. Writing—original draft: ZX, CY, FW, ZD, and YL. Writing—review and editing: ZX, CY, FW, XT, HZ, HW, ZD, and YL.

## Funding

This research was supported by the National Key R&D Program of China (2022YFA1604504), The State Key Laboratory of Space

## References

- Ambekar, R., Chittenden, M., Jasiuk, I., and Toussaint, K. C. (2012). Quantitative second-harmonic generation microscopy for imaging porcine cortical bone: Comparison to SEM and its potential to investigate age-related changes. *Bone* 50 (3), 643–650. doi:10.1016/j.bone.2011.11.013
- Bailey, S., Karsenty, G., Gundberg, C., and Vashishth, D. (2017). Osteocalcin and osteopontin influence bone morphology and mechanical properties. *Ann. N. Y. Acad. Sci.* 1409 (1), 79–84. doi:10.1111/nyas.13470
- Berezovska, O., Yildirim, G., Budell, W., Yagerman, S., Pidhaynyy, B., Bastien, C., et al. (2019). Osteocalcin affects bone mineral and mechanical properties in female mice. *Bone* 128, 115031. doi:10.1016/j.bone.2019.08.004
- Bouxsein, M. L., Boyd, S. K., Christiansen, B. A., Guldberg, R. E., Jepsen, K. J., and Müller, R. (2010). Guidelines for assessment of bone microstructure in rodents using micro-computed tomography. *J. Bone Mineral Res. Official J. Am. Soc. Bone Mineral Res.* 25 (7), 1468–1486. doi:10.1002/jbmr.141
- Camy, C., Brioché, T., Senni, K., Bertaud, A., Genovesio, C., Lamy, E., et al. (2022). Effects of hindlimb unloading and subsequent reloading on the structure and mechanical properties of Achilles tendon-to-bone attachment. *Faseb J.* 36 (10), e22548. doi:10.1096/fj.202200713R
- Chen, L., Jacquet, R., Lowder, E., and Landis, W. J. (2015). Refinement of collagen-mineral interaction: A possible role for osteocalcin in apatite crystal nucleation, growth and development. *Bone* 71, 7–16. doi:10.1016/j.bone.2014.09.021
- Chenu, C., Colucci, S., Grano, M., Zigrino, P., Barattolo, R., Zamboni, G., et al. (1994). Osteocalcin induces chemotaxis, secretion of matrix proteins, and calcium-mediated intracellular signaling in human osteoclast-like cells. *J. Cell Biol.* 127 (4), 1149–1158. doi:10.1083/jcb.127.4.1149
- Courtland, H. W., Nasser, P., Goldstone, A. B., Spevak, L., Boskey, A. L., and Jepsen, K. J. (2008). Fourier transform infrared imaging microspectroscopy and tissue-level mechanical testing reveal intraspecies variation in mouse bone mineral and matrix composition. *Calcif. Tissue Int.* 83 (5), 342–353. doi:10.1007/s00223-008-9176-8
- Cryan, J. F., Mombereau, C., and Vassout, A. (2005). The tail suspension test as a model for assessing antidepressant activity: Review of pharmacological and genetic studies in mice. *Neurosci. Biobehav. Rev.* 29 (4-5), 571–625. doi:10.1016/j.neubiorev.2005.03.009
- Desbois, C., Hogue, D. A., and Karsenty, G. (1994). The mouse osteocalcin gene cluster contains three genes with two separate spatial and temporal patterns of expression. *J. Biol. Chem.* 269 (2), 1183–1190. doi:10.1016/s0021-9258(17)42240-x
- Diegel, C. R., Hann, S., Ayturk, U. M., Hu, J. C., Lim, K.-e., Droscha, C. J., et al. (2020). An osteocalcin-deficient mouse strain without endocrine abnormalities. *PLoS Genet.* 16 (5), e1008361. doi:10.1371/journal.pgen.1008361
- Donnelly, E. (2011). Methods for assessing bone quality: A review. *Clin. Orthop. Relat. Res.* 469 (8), 2128–2138. doi:10.1007/s11999-010-1702-0

Medicine Fundamentals and Application, China Astronaut Research and Training Center (SMFA18B02, SMFA19C03, SMFA22B04), Space Medical Experiment Project of China Manned Space Program (HYZHXM01002), and the Advanced Space Medico-Engineering Research Project of China (2022SY54B0506). The funders had no role in the study design, data collection, analysis, the decision to publish, or the preparation of the manuscript.

## Acknowledgments

We thank all thirteen authors for their contribution to this work.

## Conflict of interest

The authors declare that the research was conducted in the absence of any commercial or financial relationships that could be construed as a potential conflict of interest.

## Publisher's note

All claims expressed in this article are solely those of the authors and do not necessarily represent those of their affiliated organizations, or those of the publisher, the editors and the reviewers. Any product that may be evaluated in this article, or claim that may be made by its manufacturer, is not guaranteed or endorsed by the publisher.

## Supplementary material

The Supplementary Material for this article can be found online at: <https://www.frontiersin.org/articles/10.3389/fphys.2023.1136561/full#supplementary-material>

- Ducy, P., Desbois, C., Boyce, B., Pinero, G., Story, B., Dunstan, C., et al. (1996). Increased bone formation in osteocalcin-deficient mice. *Nature* 382 (6590), 448–452. doi:10.1038/382448a0
- Faibish, D., Gomes, A., Boivin, G., Binderman, I., and Boskey, A. (2005). Infrared imaging of calcified tissue in bone biopsies from adults with osteomalacia. *Bone* 36 (1), 6–12. doi:10.1016/j.bone.2004.08.019
- Hakimimehr, D., Liu, D.M., and Troczynski, T. (2005). *In-situ* preparation of poly(propylene fumarate)-hydroxyapatite composite. *Biomaterials* 26 (35), 7297–7303. doi:10.1016/j.biomaterials.2005.05.065
- Hauschka, P. V., Lian, J. B., Cole, D., and Gundberg, C. M. (1989). Osteocalcin and matrix Gla protein: Vitamin K-dependent proteins in bone. *Physiol. Rev.* 69 (3), 990–1047. doi:10.1152/physrev.1989.69.3.990
- Hoang, Q. Q., Sicheri, F., Howard, A. J., and Yang, D. S. (2003). Bone recognition mechanism of porcine osteocalcin from crystal structure. *Nature* 425 (6961), 977–980. doi:10.1038/nature02079
- Hooshmand, S., and Arjmandi, B. H. (2009). Viewpoint: Dried plum, an emerging functional food that may effectively improve bone health. *Ageing Res. Rev.* 8 (2), 122–127. doi:10.1016/j.arr.2009.01.002
- Hosseini, S., Naderi-Manesh, H., Vali, H., Baghaban Eslaminejad, M., Azam Sayahpour, F., Sheibani, S., et al. (2019). Contribution of osteocalcin-mimetic peptide enhances osteogenic activity and extracellular matrix mineralization of human osteoblast-like cells. *Colloids Surfaces. B, Biointerfaces* 173, 662–671. doi:10.1016/j.colsurfb.2018.10.035
- Iline-Vul, T., Kulpanovich, A., Nadav-Tsubery, M., Semionov, A., Keinan-Adamsky, K., and Goobes, G. (2019). How does osteocalcin lacking  $\gamma$ -glutamic groups affect biomimetic apatite formation and what can we say about its structure in bound form? *J. Struct. Biol.* 207 (2), 104–114. doi:10.1016/j.jsb.2019.04.014
- Khrimian, L., Obri, A., Ramos-Brossier, M., Rouseaud, A., Moriceau, S., Nicot, A.-S., et al. (2017). Gpr158 mediates osteocalcin's regulation of cognition. *J. Exp. Med.* 214 (10), 2859–2873. doi:10.1084/jem.20171320
- Komori, T. (2020). Functions of osteocalcin in bone, pancreas, testis, and muscle. *Int. J. Mol. Sci.* 21 (20), 7513. doi:10.3390/ijms21207513
- Lai, C. C., Lo, C. Y., Hsieh, T. H., Tsai, W. S., Nguyen, D. H., and Ma, Y. R. (2016). Ligand-driven and full-color-tunable fiber source: Toward next-generation clinic fiber-endoscope tomography with cellular resolution. *ACS Omega* 1 (4), 552–565. doi:10.1021/acsomega.6b00146
- Lambert, L. J., Challa, A. K., Niu, A., Zhou, L., Tucholski, J., Johnson, M. S., et al. (2016). Increased trabecular bone and improved biomechanics in an osteocalcin-null rat model created by CRISPR/Cas9 technology. *Dis. Models Mech.* 9 (10), 1169–1179. doi:10.1242/dmm.025247
- Lee, A. J., Hodges, S., and Eastell, R. (2000). Measurement of osteocalcin. *Ann. Clin. Biochem.* 37 (4), 432–446. doi:10.1177/000456320003700402
- Lee, N. K., Sowa, H., Hinoi, E., Ferron, M., Ahn, J. D., Confavreux, C., et al. (2007). Endocrine regulation of energy metabolism by the skeleton. *Cell* 130 (3), 456–469. doi:10.1016/j.cell.2007.05.047
- Li, B., Zhao, J., Ma, J., Chen, W., Zhou, C., Wei, W., et al. (2021). Cross-talk between histone and DNA methylation mediates bone loss in hind limb unloading. *J. Bone Min. Res.* 36 (5), 956–967. doi:10.1002/jbmr.4253
- Li, Y. P., Chen, W., and Stashenko, P. (1995). Characterization of a silencer element in the first exon of the human osteocalcin gene. *Nucleic Acids Res.* 23 (24), 5064–5072. doi:10.1093/nar/23.24.5064
- Lian, J. B., and Gundberg, C. M. (1988). Osteocalcin. Biochemical considerations and clinical applications. *Clin. Orthop. Relat. Res.* 226 (226), 267–291. doi:10.1097/00003086-198801000-00036
- López Barreiro, D., Martín-Moldes, Z., Blanco Fernández, A., Fitzpatrick, V., Kaplan, D. L., and Buehler, M. J. (2022). Molecular simulations of the interfacial properties in silicohydroxyapatite composites. *Nanoscale* 14 (30), 10929–10939. doi:10.1039/d2nr01989b
- Makowski, A. J., Patil, C. A., Mahadevan-Jansen, A., and Nyman, J. S. (2013). Polarization control of Raman spectroscopy optimizes the assessment of bone tissue. *J. Biomed. Opt.* 18 (5), 55005. doi:10.1117/1.JBO.18.5.055005
- Manolagas, S. C. (2020). Osteocalcin promotes bone mineralization but is not a hormone. *PLoS Genet.* 16 (6), e1008714. doi:10.1371/journal.pgen.1008714
- McGuigan, F., Kumar, J., Ivaska, K. K., Obrant, K. J., Gerdhem, P., and Åkesson, K. (2010). Osteocalcin gene polymorphisms influence concentration of serum osteocalcin and enhance fracture identification. *J. bone mineral Res.* 25 (6), 1392–1399. doi:10.1002/jbmr.32
- Mera, P., Laue, K., Ferron, M., Confavreux, C., Wei, J., Galán-Díez, M., et al. (2016). Osteocalcin signaling in myofibers is necessary and sufficient for optimum adaptation to exercise. *Cell Metab.* 23 (6), 1078–1092. doi:10.1016/j.cmet.2016.05.004
- Moriishi, T., and Komori, T. (2020). Lack of reproducibility in osteocalcin-deficient mice. *PLoS Genet.* 16 (6), e1008939. doi:10.1371/journal.pgen.1008939
- Moriishi, T., Ozasa, R., Ishimoto, T., Nakano, T., Hasegawa, T., Miyazaki, T., et al. (2020). Osteocalcin is necessary for the alignment of apatite crystallites, but not glucose metabolism, testosterone synthesis, or muscle mass. *PLoS Genet.* 16 (5), e1008586. doi:10.1371/journal.pgen.1008586
- Oury, F., Khrimian, L., Denny, C. A., Gardin, A., Chamouni, A., Goeden, N., et al. (2013). Maternal and offspring pools of osteocalcin influence brain development and functions. *Cell* 155 (1), 228–241. doi:10.1016/j.cell.2013.08.042
- Oury, F., Sumara, G., Sumara, O., Ferron, M., Chang, H., Smith, C. E., et al. (2011). Endocrine regulation of male fertility by the skeleton. *Cell* 144 (5), 796–809. doi:10.1016/j.cell.2011.02.004
- Paschalis, E. P., Gamsjaeger, S., and Klaushofer, K. (2017). Vibrational spectroscopic techniques to assess bone quality. *Osteoporos. Int.* 28 (8), 2275–2291. doi:10.1007/s00198-017-4019-y
- Poundarik, A. A., Boskey, A., Gundberg, C., and Vashishth, D. (2018). Biomolecular regulation, composition and nanoarchitecture of bone mineral. *Sci. Rep.* 8 (1), 1191. doi:10.1038/s41598-018-19253-w
- Prabhakaran, M. P., Venugopal, J., and Ramakrishna, S. (2009). Electrospun nanostructured scaffolds for bone tissue engineering. *Acta Biomater.* 5 (8), 2884–2893. doi:10.1016/j.actbio.2009.05.007
- Rho, J. Y., Kuhn-Spearing, L., and Zioupos, P. (1998). Mechanical properties and the hierarchical structure of bone. *Med. Eng. Phys.* 20 (2), 92–102. doi:10.1016/s1350-4533(98)00007-1
- Terajima, M., Perdivara, I., Sricholpech, M., Deguchi, Y., Pleshko, N., Tomer, K. B., et al. (2014). Glycosylation and cross-linking in bone type I collagen. *J. Biol. Chem.* 289 (33), 22636–22647. doi:10.1074/jbc.M113.528513
- Tsao, Y.-T., Huang, Y.-J., Wu, H.-H., Liu, Y.-A., Liu, Y.-S., and Lee, O. K. (2017). Osteocalcin mediates biomineralization during osteogenic maturation in human mesenchymal stromal cells. *Int. J. Mol. Sci.* 18 (1), 159. doi:10.3390/ijms18010159
- Wang, Y., Morsali, R., Dai, Z., Minary-Jolandan, M., and Qian, D. (2020). Computational nanomechanics of noncollagenous interfibrillar interface in bone. *ACS Appl. Mater Interfaces* 12 (22), 25363–25373. doi:10.1021/acami.0c01613
- Weinreb, M., Shinar, D., and Rodan, G. A. (1990). Different pattern of alkaline phosphatase, osteopontin, and osteocalcin expression in developing rat bone visualized by *in situ* hybridization. *J. Bone Min. Res.* 5 (8), 831–842. doi:10.1002/jbmr.5650050806
- Wronski, T. J., and Morey-Holton, E. R. (1987). Skeletal response to simulated weightlessness: a comparison of suspension techniques. *Aviat. Space Environ. Med.* 58 (1), 63–68.
- Yadav, V. K., Berger, J. M., Singh, P., Nagarajan, P., and Karsenty, G. (2022). Embryonic osteocalcin signaling determines lifelong adrenal steroidogenesis and homeostasis in the mouse. *J. Clin. Investigation* 132 (4), e153752. doi:10.1172/JCI153752
- Zhang, H., Chen, J., Wang, H., Lu, X., Li, K., Yang, C., et al. (2020). Serum metabolomics associating with circulating MicroRNA profiles reveal the role of miR-383-5p in rat Hippocampus under simulated microgravity. *Front. Physiology* 11, 939. doi:10.3389/fphys.2020.00939
- Zlotnick, H. M., Locke, R. C., Hemdev, S., Stoeckl, B. D., Gupta, S., Peredo, A. P., et al. (2022). Gravity-based patterning of osteogenic factors to preserve bone structure after osteochondral injury in a large animal model. *Biofabrication* 14 (4), 044101. doi:10.1088/1758-5090/ac79cd
- Zoch, M. L., Clemens, T. L., and Riddle, R. C. (2016). New insights into the biology of osteocalcin. *Bone* 82, 42–49. doi:10.1016/j.bone.2015.05.046